Method for the synthesis of CrO_2 at ambient pressure and temperature

H. Ye
College of Chemistry and Chemical Engineering, Central-South University, Changsha 410083, People's Republic of China

Q. Zhang and F. Saito
Institute of Multidisciplinary Research for Advanced Materials, Tohoku University, Sendai 980-8577, Japan

B. Jeyadevan[a] and K. Tohji
Department of Geoscience and Technology, Tohoku University, Sendai 980-8579, Japan

M. Tsunoda
Department of Electronic Engineering, Tohoku University, Sendai 980-8579, Japan

(Presented on 12 November 2002)

In this article, we report the synthesis of metastable chromium dioxide at ambient temperature and pressure. The formulation of this method is based on the fact that the CrO_2 particles used in magnetic recording tapes are chemically unstable and react with the organic binder, leading to a disproportionate reaction that produces nonmagnetic Cr(III)OOH and $H_2Cr(VI)O_4$ compounds. This suggests that it is also possible to synthesize CrO_2 by reacting Cr(III) with Cr(VI) under appropriate conditions. Thus, metastable chromium dioxide (CrO_2) powder was synthesized by mechanically grinding a mixture of CrO_3 and $Cr(OH)_3$ to induce a solid–solid reaction at atmospheric temperature and pressure. The characteristics of the product obtained after mechanical grinding of the above mixture depended on parameters such as the preparation conditions for the starting material $Cr(OH)_3$, the grinding time, the rotational speed of the mill and the mole ratio of CrO_3 and $Cr(OH)_3$. An x-ray diffraction pattern of the product obtained under optimum conditions was in excellent agreement with the profile of CrO_2. Furthermore, the powder was strongly ferromagnetic, with saturation magnetization of 63 emu/g in an applied field of 1 T. © *2003 American Institute of Physics.* [DOI: 10.1063/1.1555988]

I. INTRODUCTION

Of several oxidation states of chromium, CrO_2 is the only chromium oxide that is strongly ferromagnetic at room temperature (Cr^{4+} is a $3d^2$ ion). And this has been of some interest technologically as a magnetic recording medium.[1] However, CrO_2 is metastable at atmospheric pressure and temperature and synthesis with these requires stringent conditions.[2,3] Recently, it was reported that CrO_2 could be prepared by decomposing $Cr(NO_3)_3$ impregnated in a polycrystalline rutile (TiO_2) support under ambient pressure.[4] Another report claimed that CrO_2 could be produced by reducing CrO_3 with NH_4I/NH_4Br at temperatures between 120 and 150 °C and annealing the solid product at temperatures below the decomposition point of CrO_2.[5] However, further simplification of the synthesis process is very much desired to study the intrinsic properties of this oxide and also the effect of potential dopants that could enhance the above properties. In this article, we report a method by which to synthesize CrO_2 by reacting Cr(III) with Cr(VI) compounds mechanochemically. It was found that CrO_2 can be synthesized by grinding a mixture of CrO_3 and $Cr(OH)_3 \cdot nH_2O$ at ambient pressure and temperature conditions. The product obtained was strongly ferromagnetic and its x-ray diffraction pattern was in excellent agreement with the pattern reported for CrO_2 in the literature.

[a]Electronic mail: jeya@ni4.earth.tohoku.ac.jp

II. EXPERIMENT

The raw materials for Cr(VI) and Cr(III) were reagent grade CrO_3 and $Cr(OH)_3 \cdot nH_2O$, respectively (supplied by Wako Chemical Co. Ltd., Japan). A planetary ball mill (Fritch Pulverisette-7, Germany) with two zirconia vials was used to mechanically mill the mixture of reagents. The inner diameter and volume of each vial were 80 mm and 45 cm^3, respectively. In our experiments, zirconia balls 15 mm in diameter were used as the grinding media, and about 2 g of a Cr(VI) and Cr(III) mixture was used as the starting material. The ball/powder ratio was about 35:1. The phases present in the ground products were identified by x-ray diffraction (XRD) (Cu-MultiFlux, Rigaku, Japan) analysis. The magnetic properties were determined by a vibrating sample magnetometer (VSM) (Tamakawa model TM-VSM1230-HHHS). Thermal gradient/differential thermal gradient (TG/DTG) analysis of the samples was performed at various stages of grinding in a thermal balance (Rigaku Thermoplus TG-8120). The morphology of the product was monitored by a scanning electron microscope (SEM) (Hitachi S-4100).

III. RESULTS AND DISCUSSION

It has been reported[5] that the CrO_2 particles used in magnetic recording tapes are chemically unstable and react with the organic binder, leading to a noticeable loss in magnetization. Although the mechanism is yet to be completely

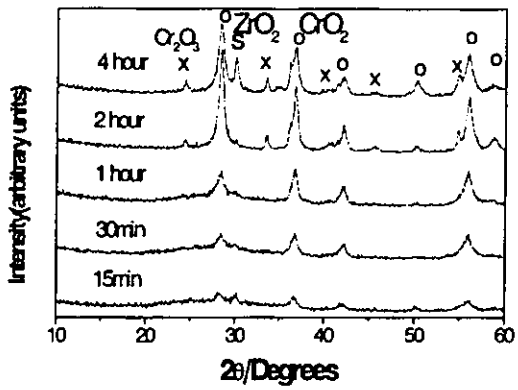

FIG. 1. X-ray diffraction patterns of ground products obtained for different grinding times.

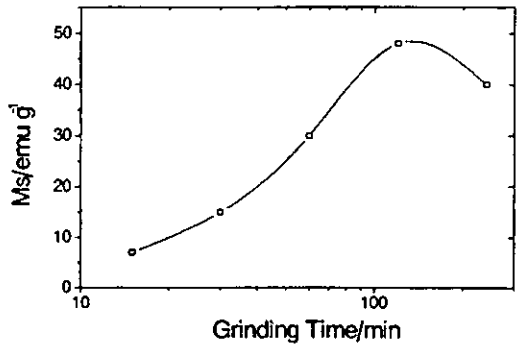

FIG. 2. Magnetization at 1 T of ground products obtained for different grinding times.

understood, it is well established that a disproportionate reaction produces nonmagnetic compounds given by

$$3CrO_2 + 2H_2O = 2CrOOH + H_2CrO_4. \quad (1)$$

It can be noticed that part of $Cr(IV)O_2$ is converted into $Cr(III)OOH$ and the rest into $H_2Cr(VI)O_4$. This implies that it is also possible to synthesize CrO_2 by reacting Cr(III) with Cr(VI) under appropriate conditions.

According to the reverse reaction in Eq. (1), an oxidizing agent, H_2CrO_4, and a reducing agent, CrOOH, were necessary to synthesize CrO_2. Here, we selected CrO_3, which can form H_2CrO_4 easily in the presence of water. Furthermore, CrO_3 has a high electron affinity (EA) and could act as a strong oxidizing agent. As for CrOOH, $Cr(OH)_3 \cdot nH_2O$ was annealed at a predetermined temperature for a specified period of time. Based on the reaction $Cr^{6+} + 2Cr^{3+} = 3Cr^{4+}$, the mixture of CrO_3 and $Cr(OH)_3$ with molar ratio equivalent of 1:2 was ground in the mill.

The XRD patterns of the ground powders obtained for different grinding times are shown in Fig. 1. The diffraction peaks corresponding to CrO_2 began to appear within 15 min of grinding, and their intensities rose according to the amount of grinding. However, it should be noted that for grinding periods longer than 2 h, peaks corresponding to Cr_2O_3 and ZrO_2 (grinding media) began to appear. On the other hand, the peak intensities of CrO_2 also depended on the rotation speed of the mill for a fixed grinding time of 2 h, and reached a maximum at 700 rpm.

The saturation magnetization M_s in 1 T applied field as a function of the grinding time is shown in Fig. 2. The ferromagnetic fraction in the ground powder increased with grinding time with M_s reaching a maximum of 48 emu/g after 2 h. On the other hand, the M_s of the products obtained for different rotation speeds reached a maximum of 48 emu/g at 700 rpm. Thus, the optimum grinding time and rotation speed were fixed as 2 h and 700 rpm, respectively.

Based on the above results, it is reasonable to assume that the following solid–solid reaction has taken place during milling:

$$CrO_3 + 2Cr(OH)_3 = 3CrO_2 + 3H_2O. \quad (2)$$

However, diffraction peaks corresponding to Cr_2O_3 appeared for powders ground for 2 h or more, irrespective of the rotation speed. The formation of Cr_2O_3 could have been due to overannealing of $Cr(OH)_3 \cdot nH_2O$, nonstoichiometric ratio between the starting material in Eq. (2) and/or the reduction of CrO_2. In order to inhibit the formation of Cr_2O_3, milling was carried out under varying initial molar ratios of CrO_3:$Cr(OH)_3$ and the XRD patterns of the ground product are given in Fig. 3. It is clear that the intensity of the peak corresponding to Cr_2O_3 was due to the nonstoichiometry of reaction (2). The addition of CrO_3 in quantities slightly over the stoichiometric requirement effectively inhibited the formation of Cr_2O_3 in the ground product. It is believed that when there was an excess of $Cr(OH)_3$, dehydration of it would form Cr_2O_3 according to the reaction.

$$2Cr(OH)_3 = Cr_2O_3 + 3H_2O. \quad (3)$$

The SEM analysis of the samples ground for different durations clearly showed the progress of size reduction in the mechanochemical reaction. Although the particle size of the ground powder was reduced to submicron size with the grinding time, agglomeration of the particles became very pronounced as shown in Fig. 4. TG/DTG analysis of the sample ground at 700 rpm for 2 h revealed that the product was thermally stable until 400 °C and the loss of weight below this temperature was due to the loss of water. However, at temperatures higher than 400 °C, the CrO_2 decomposed

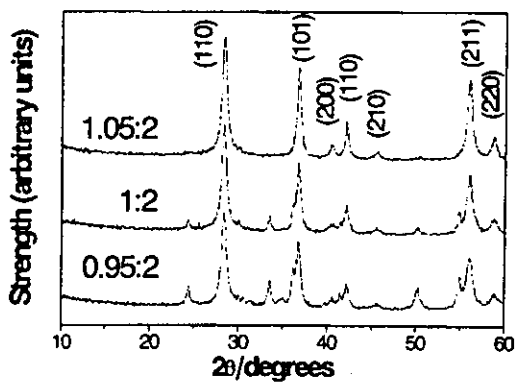

FIG. 3. X-ray diffraction patterns of ground products obtained for different CrO_3 and $Cr(OH)_3 \cdot nH_2O$ mole ratios.

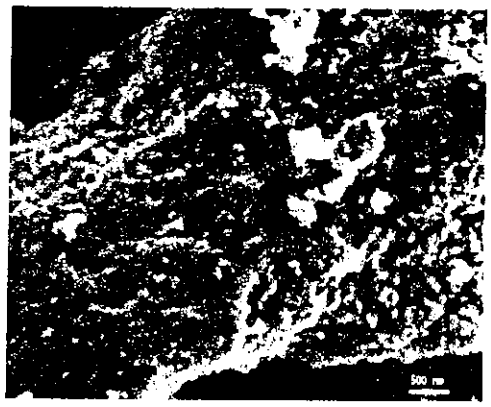

FIG. 4. SEM micrograph of the CrO_2 sample synthesized by ball milling for 2 hours at 700 rpm.

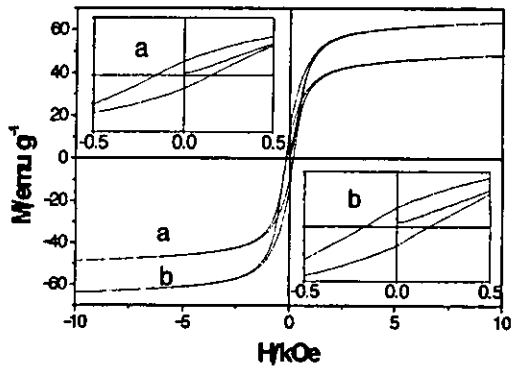

FIG. 5. Magnetic hysteresis loops (a) before and (b) after annealing the product obtained by grinding a CrO_3 and $Cr(OH)_3 \cdot nH_2O$ mixture with ratio of 1.05:2 for 2 h at 700 rpm.

into Cr_2O_3 and the corresponding weight loss was recorded. This was confirmed by XRD of the sample treated at 500 °C. It is known that bound water in raw material of $CrOOH \cdot nH_2O$ is necessary in order for it to react with CrO_3 and form CrO_2 magnetic powder. And 16% of the water is contained in $Cr(OH)_3$. Therefore, the saturation magnetization of the powder could be improved by drying it at a specific temperature. Thus the sample was annealed at 300 °C for 5 h. The magnetic hysteresis loops of the samples before and after drying are shown in Fig. 5. The magnetization improved by about 30% and the M_s increased from 48 to 63 emu/g and H_c from 128 to 190 Oe. However, the change in weight was only 6%. The additional increase in magnetization is believed to be due to CrO_2 crystal grain growth induced by thermal annealing.

IV. CONCLUSION

Metastable CrO_2 magnetic powder was synthesized by grinding a mixture of CrO_3 and $CrOOH \cdot nH_2O$. The XRD analysis and the magnetic properties of the powder confirmed the formation of CrO_2. The quality of the product depended on the mole ratio of CrO_3 and $CrOOH \cdot nH_2O$, the grinding time, and the speed of rotation of the mill. Further enhancement of the magnetic properties of the powder was obtained by annealing the sample at temperatures below the decomposition temperature of CrO_2. This synthesis method is of practical importance for its simplicity, especially since there is no requirement for the high pressure used in traditional methods.

ACKNOWLEDGMENT

The Education Ministry of China is gratefully acknowledged for its financial support.

[1] J. Kubota, J. Am. Ceram. Soc. **44**, 239 (1961).
[2] B. L. Chamberland, CRC Crit. Rev. Solid State Mater. Sci. **7**, 1 (1977).
[3] R. G. Egdell, E. Brand, and D. Kellett, J. Mater. Chem. **9**, 2717 (1999).
[4] K. Ramesha and J. Gopalakrishnan, Chem. Commun. (Cambridge) **1999**, 1173 (1999).
[5] G. Basile, G. C. Boero, F. Garbassi, E. M. Ceresa, and F. Montino, MRS Bull. **17**, 1197 (1982).

ACADEMIC PRESS

Available online at www.sciencedirect.com

SCIENCE DIRECT®

Journal of Colloid and Interface Science 263 (2003) 80–83

JOURNAL OF Colloid and Interface Science

www.elsevier.com/locate/jcis

Synthesis of size-controlled cobalt ferrite particles with high coercivity and squareness ratio

C.N. Chinnasamy, M. Senoue, B. Jeyadevan,* Oscar Perales-Perez, K. Shinoda, and K. Tohji

Department of Geoscience and Technology, Tohoku University, Sendai 980-8579, Japan

Received 19 September 2002; accepted 5 March 2003

Abstract

Cobalt ferrite particles with diameters ranging from a few micrometer to about 15 nm were synthesized using a modified oxidation process. The fine control of the particle size was achieved by introducing various concentrations of Fe^{3+} ions at the beginning of the reaction. Among the particle sizes obtained by using this method, particles with a grain size of about 36 nm showed a magnetization (M_s) of 64 emu/g and a maximum coercivity (H_c) of 2020 Oe at room temperature. The corresponding squareness ratio was found to be 0.53.

Keywords: Cobalt ferrite; Coprecipitation; Colloids; Ferrous oxidation by nitrate; Nanoparticles; Magnetic characterization

1. Introduction

There is an increasing interest in magnetic ferrite nanoparticles because of their broad applications in several technological fields including permanent magnets, magnetic fluids, magnetic drug delivery, microwave devices, and high-density information storage [1–3]. Though γ-Fe_2O_3 and Co-doped magnetites are already being used in recording media, renewed interest is being shown to cobalt ferrite ($CoFe_2O_4$), which is considered a potential candidate for high-density recording. This is because of its magnetic properties such as strong anisotropy and hence high coercivity at room temperature and moderate saturation magnetization, along with good mechanical hardness and chemical stability. These characteristics, and also the fact that the magnetic properties of the ferrite particles are strongly dependent on their size, justify any effort to produce size-tuned cobalt ferrite particles with diameters ranging from the superparamagnetic threshold of 10 nm to the critical single-domain size of 70 nm [4,5]. The $CoFe_2O_4$ prepared by the conventional coprecipitation method [6] has resulted in particle sizes ranging from 5 to 25 nm and their magnetization, M_s, and coercivity, H_c, are about 60 emu/g and 550 Oe, respectively. The poor magnetic properties are due to the presence of a large fraction of superparamagnetic particles. In spite of the development of a variety of solution-based synthesis routes, the production of cobalt ferrite particles with the desirable size and magnetic properties is still a challenge.

In a recent report, the authors developed a method to achieve a fine-tuning of the size of cobalt ferrite nanoparticles. This method has made possible the production of nonaggregated primary particles of size of 40 nm exhibiting a coercivity value as high as 4.3 kOe at 300 K [7]. The as-synthesized powder, i.e., without size selection, showed a H_c of 2.9 kOe only due to the presence of a significant fraction of superparamagnetic particles.

On the other hand, Tamura and Matijević [8] proposed a method to produce cobalt ferrite particles having different morphology. Their method was based on the development of the ferrite structure from ferrous hydroxide gels in the presence of a mild oxidizing agent. The as-prepared cobalt ferrite particles were submicrometer in size and exhibited various compositions depending on the synthesis conditions. Though the magnetic properties of these particles were not reported, it is understood that generally the micrometer-size particles have small coercivities compared to that of single domain size particles. Taking their approach as a reference line and with an attempt to improve the room-temperature magnetic properties of the nanometer-sized cobalt ferrite particles, the present work explores the possibilities of further lowering the size of the ferrite particles by restricting the

* Corresponding author.
E-mail address: jeya@ni4.earth.tohoku.ac.jp (B. Jeyadevan).

0021-9797/03/$ – see front matter
doi:10.1016/S0021-9797(03)00258-3

particle growth to the range from 10 to 100 nm by modifying the oxidation method [8] using various concentrations of Fe^{3+} ions at the beginning of the reaction to induce the formation of nuclei at early stages and promote heterogeneous nucleation.

2. Experimental

2.1. Materials

All reagents were of analytical grade and were used without any further purification. Required weights of $FeSO_4 \cdot 7H_2O$, $Fe_2(SO_4)_3 \cdot nH_2O$, and $CoSO_4 \cdot 6H_2O$ salts were used to achieve a Fe/Co mole ratio of 2. Potassium nitrate, KNO_3, was used as a mild oxidizing agent. The intermediate compound was precipitated by contacting the metals and nitrate solutions with suitable amounts of sodium hydroxide (NaOH).

2.2. Synthesis of cobalt ferrite

Prior to the precipitation and oxidation experiments, nitrogen (N_2) gas was purged into the aqueous solutions of NaOH in order to minimize the content of residual dissolved oxygen. To this oxygen-free solution, 0.085 M of ferrous and 0.0425 M of cobalt sulfate salts were added. In all batches of the experiments, the total concentration of iron ions was kept constant but the Fe(III)/Fe(II) mole ratio was adjusted by dissolving suitable amounts of ferric and ferrous sulfate salts in the starting solutions. The reaction vessel containing the mixture of iron and cobalt ions was then contacted with NaOH solution. The effect of concentration of the oxidizing nitrate ions on particle size and morphology was evaluated by dissolving variable amounts of KNO_3 salt into the metal solutions. The aqueous suspension containing the ferrite precursor, considered to be a mixture of cobalt and iron hydroxides, was heated up to $93 \pm 2\,^{\circ}C$ under a continuous purging of nitrogen gas to prevent the atmospheric oxidation of the ferrous species. A reaction time of 2 h was found to be sufficient to convert the intermediate hydroxides into the ferrite compound.

2.3. Characterization

The X-ray diffraction (XRD) analyses of the synthesized ferrite powders were carried out in a RIGAKU X-ray diffractometer using CuK_α radiation. The particle morphology was examined by using a scanning electron microscope (SEM, Hitachi S-4100) and a high-resolution transmission electron microscope (HRTEM, Hitachi HF-2000). The magnetization measurements were carried out at room temperature by using a Vibrating Sample Magnetometer (Model TM-VSM1230-HHHS) with a maximum applied field of 1.5 T.

3. Results and discussion

Tamura and Matijević [8] have studied the effect of Fe/Co mole ratio in the starting solutions on the particle size. They found that the cobalt ferrite particles were spherical with diameters ranging from a few micrometers to about 100 nm depending upon the Fe/Co mole ratio. The reaction time required for the complete conversion of the hydroxides to ferrite was nearly 20 h. In our approach, ferrous species were partially oxidized by nitrate ions to give $CoFe_2O_4$ particles of well-defined morphology with a fairly uniform and narrow size distribution.

It is also found that the properties of the particles are dependent on the concentration of the reacting components, the pH, and the nature of anions and cations in the aging system. In view of this and also in order to optimize the preparation conditions, leading to a further decrease in the size of cobalt ferrite particles to the range from 10 to 70 nm, the effect of the following factors were systematically investigated: concentration of oxidizing (NO_3^-) species, stoichiometric excess of precipitating OH^- ions with respect to the requirement for the hydroxide formation and the Fe(III)/Fe(II) mole ratio in starting solutions. The basic idea is to explore the possibilities to enhance the nucleation rate by controlling the formation of ferric entities in the system and restrict the particle growth and/or aggregation by increasing the electrostatic repulsive force between the negatively charged particle surfaces, an effect expected with excess of OH^- ions.

3.1. Effect of KNO_3 and NaOH concentration

On the consideration that the higher the availability of the oxidizing agent the larger and faster the generation of ferric species, experiments with various concentrations of KNO_3 (0.015–0.03 M) were undertaken. The XRD patterns corresponding to the particles produced at different concentrations of nitrate ions and with 2 h of reaction time showed only $CoFe_2O_4$ phase with an average grain size of 52 nm irrespective of the KNO_3 concentration. The magnetic measurements gave 71 emu/g for M_s, 1360 Oe for H_c, and a squareness ratio of 0.61 for the cobalt ferrite produced in the presence of 0.02 M KNO_3 in starting solutions. The high squareness ratio is attributed to a small volume fraction of superparamagnetic particles. Above 0.02 M of KNO_3, the oxidation potential might have reached a saturation value that caused the oxidizing conditions to be more or less constant. On this basis, 0.02 M of KNO_3 was considered the optimum amount of oxidizing agent to obtain well-crystallized $CoFe_2O_4$ particles.

On the other hand, the effect of an excess concentration of OH^- ions was investigated between 0.225 and 0.56 M for two levels of KNO_3, namely, 0.02 and 0.03 M. Though the stoichiometric requirement of NaOH was 0.255 M for the total moles of cobalt and ferrous ions, $CoFe_2O_4$ particles were synthesized in the presence of 0.225, 0.25, 0.312, and

0.375 M of OH^- ions for a fixed concentration of 0.02 M of KNO_3. When the OH^- concentration was less than the stoichiometric requirement, the reaction was not completed within 2 h and also the FeOOH phase was detected in the XRD analysis along with the ferrite phase. No peaks corresponding to cobalt hydroxide were identified in the XRD pattern. The XRD data suggest that some of the iron, probably generated by incomplete precipitation of cobalt ions, was not incorporated into the ferrite structure; instead it was oxidized and precipitated as an isolated phase. In turn, the cobalt ferrite particles produced at OH^- concentrations above the stoichiometric requirement were of cubic morphology with well-defined crystal habits, which could be due to the direct crystal growth mechanism [9]. The average crystallite size was estimated to be about 58 nm. The SEM observations clearly showed the aggregation of primary particles to give large and irregular polycrystals. This effect could be attributed to the aggregation of extremely small primary particles that nucleated inside the hydroxide precursor, with their subsequent growth taking place through the contact-recrystallization mechanism [10]. Similar trends in particle size were observed for the experiments carried out in the presence of 0.03 M of KNO_3. Therefore, the increase of OH^- concentration beyond the stoichiometric concentration does not help to synthesize $CoFe_2O_4$ particles below 70 nm. Furthermore, the coercivity of these particles at 300 K was as low as 1300 Oe.

3.2. Effect of the concentration of ferric ions

The oxidation of ferrous ions would promote the ferrite nucleation rate and lead to a decrease in the particle size. This could be achieved either through stronger oxidizing agents or the addition of ferric ions from the very beginning. In view of this, the experimental conditions were set up to synthesize cobalt ferrite particles in the presence of ferrous and ferric ions in starting solutions. The percentage values of ferric ions were 15, 20, 25, 35, and 50 of the total iron concentration. The total Fe/Co mole ratio was kept constant as 2:1. The concentration of NaOH was adjusted depending on the stoichiometric requirements for the metal ion mixture.

All the products synthesized under these conditions consisted of the ferrite phase. Under these experimental conditions, the coexistence of ferrous and ferric ions from the beginning would give an equal probability for the formation of both magnetite and cobalt ferrite. However, the peak positions at high angles of the XRD patterns and the calculated lattice parameters confirmed the presence of $CoFe_2O_4$. This fact suggests that the formation of $CoFe_2O_4$ might have been kinetically favored over the magnetite formation. Also, the concentration of ferric ions in the starting solution had a marked effect on the average grain size estimated from the (311) XRD peak, as seen from the data in Table 1. The SEM and TEM micrographs of the ferrite powders produced for various concentrations of ferric ions are shown in Fig. 1. It is evident from these micrographs that the particle size of the ferrite powders decreased with increase in ferric ion concentration. The addition of ferric ions led to a decrease in the ferrite particle size that dropped from 100 to less than 15 nm when the ferric ion fraction in the starting solutions

Table 1
The effect of Fe^{3+} ion concentrations on the structural and magnetic properties of the $CoFe_2O_4$ at 300 K

Fe^{3+} conc. (%)	Average grain size from XRD (nm)	Particle size from SEM and TEM (nm)	M_s (emu/g)	H_c (Oe)	Sq. ratio (M_r/M_s)
0	53	100–110	71	1360	0.61
15	30	60–90	60	1150	0.41
20	28	60–90	64	1870	0.51
25	30	60–70	69	1860	0.51
35	36	30–40	64	2020	0.53
50	14	15–20	61	631	0.30

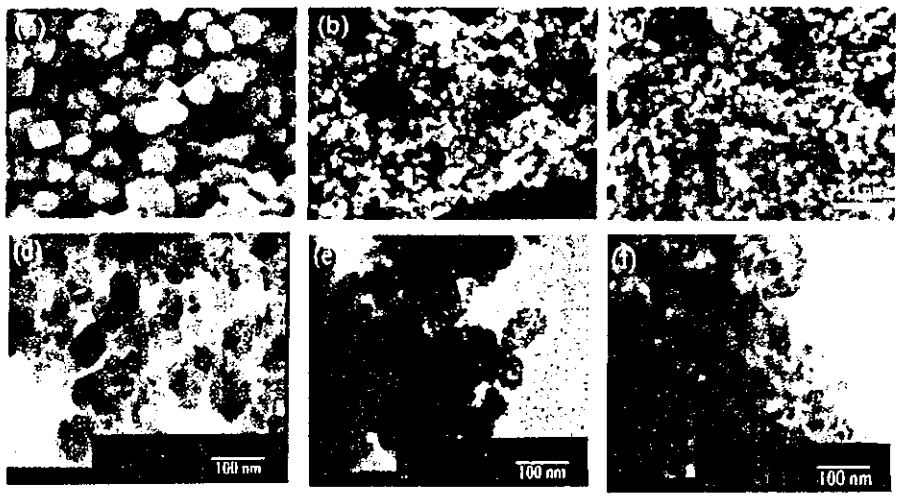

Fig. 1. The SEM and TEM micrographs of $CoFe_2O_4$ particles synthesized under various ferric ion concentrations. The Fe^{3+}/Fe^{2+} ratios are (a) 0, (b) 0.15, (c) 0.20, (d) 0.25, (e) 0.35, and (f) 0.50.

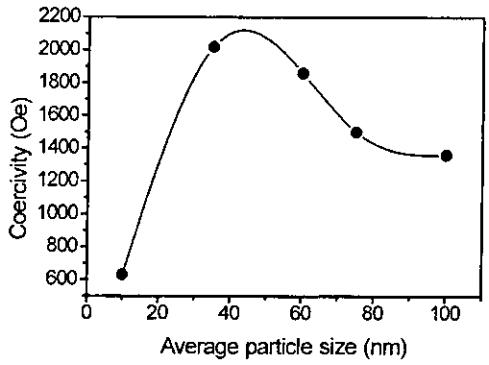

Fig. 2. The relationship between the average particle size and the coercivity of $CoFe_2O_4$ at 300 K (the continuous line is guide to the eye).

changed from 0 to 50%, respectively. The discrepancy in the particle sizes obtained from XRD and SEM measurements especially for the powders produced at lower concentrations of ferric ions suggests that at higher ferric ion concentrations the particles are probably single crystals while they become polycrystals at lower concentrations. The coercivity and the magnetization of the ferrite synthesized at the 50% ferric ion concentration in the starting solution are comparable to the values reported for cobalt ferrite produced by the conventional coprecipitation method [6].

Table 1 also shows the results of the magnetization measurements of the ferrite products. The magnetization is between 60 and 71 emu/g. The relationship between the average particle size and coercivity is shown in Fig. 2. The coercivity first increases as the particle size decreases, reaches a maximum value of 2020 Oe between 30–40 nm and then decreases for any further decrease in particle size. The squareness ratio of the particle exhibiting the highest coercivity is 0.53. The value of 2020 Oe for the coercivity at 300 K is the highest reported so far for this ferrite produced through the low temperature synthesis technique. As the single domain size of cobalt ferrite is reported to be around 70 nm [5], the magnetization mechanism for particles below and above the single domain size will be different. This mechanism also contributes to the variation observed in the coercivity values.

4. Conclusions

Cobalt ferrite particles with diameters ranging from a few microns to about 15 nm have been synthesized by using the modified oxidation method. The effect of the concentration of the oxidizing agent namely, the nitrate ions, and the addition of ferric ions from the very beginning of the reaction on the size and magnetic properties of the particles has been studied in detail. The cobalt ferrite particles synthesized under optimum conditions had an average grain size of 36 nm and showed coercivity as high as 2020 Oe and squareness ratio of 0.53 under a 1.5 T applied magnetic field at room temperature.

References

[1] A. Goldman, Modern Ferrite Technology, Van Nostrand–Reinhold, New York, 1990.
[2] B.M. Berkovsky, V.F. Medvedev, M.S. Krakov, Magnetic Fluids: Engineering Applications, Oxford Univ. Press, Oxford, 1993.
[3] Y. Kitamoto, S. Kantake, S. Shirasaki, F. Abe, M. Naoe, J. Appl. Phys. 85 (1999) 4708.
[4] D.J. Dunlop, Philos. Mag. 19 (1969) 329.
[5] A.E. Berkowitz, W.J. Schuele, J. Appl. Phys. 30 (1959) 134S.
[6] T. Sato, T. Iijima, M. Seki, N. Inagaki, J. Magn. Magn. Mater. 65 (1987) 252.
[7] C.N. Chinnasamy, B. Jeyadevan, O. Perales-Perez, K. Shinoda, K. Tohji, A. Kasuya, IEEE Trans. Magn. 38 (2002) 2640.
[8] H. Tamura, E. Matijević, J. Colloid Interface Sci. 90 (1982) 100.
[9] T. Sugimoto, E. Matijević, J. Colloid Interface Sci. 74 (1980) 227.
[10] T. Sugimoto, T. Yamaguchi, J. Cryst. Growth 34 (1976) 253.

Unusually high coercivity and critical single-domain size of nearly monodispersed $CoFe_2O_4$ nanoparticles

C. N. Chinnasamy, B. Jeyadevan,[a] K. Shinoda, and K. Tohji
Graduate School of Environmental Studies, Tohoku University, Aoba-ku, Sendai 980-8579, Japan

D. J. Djayaprawira and M. Takahashi
Department of Electronic Engineering, Tohoku University, Aoba-ku, Sendai 980-8579, Japan

R. Justin Joseyphus and A. Narayanasamy
Materials Science Center, Department of Nuclear Physics, University of Madras, Guindy Campus, Chennai-600 025, India

(Received 11 June 2003; accepted 13 August 2003)

Nearly monodispersed $CoFe_2O_4$ nanoparticles with average sizes between 8 and 100 nm were synthesized by using seed-mediated growth dominant coprecipitation and modified oxidation methods. X-ray diffraction and Mössbauer spectroscopy analyses confirmed the spinel phase and a stoichiometric composition of $(Co_{0.25}Fe_{0.75})[Co_{0.75}Fe_{1.25}]O_4$ for powders with different particle diameters. Rotational hysteresis loss (W_r) analysis showed an average switching field (H_p) of 17 kOe and a magnetic anisotropy field (H_k) of 38 kOe for the 40 nm $CoFe_2O_4$ particles. The corresponding magnetocrystalline anisotropy energy constant (K) was about 5.1×10^6 erg/cc. The H_c and H_p results suggest that the critical single-domain size of $CoFe_2O_4$ is about 40 nm. The room temperature coercivity (H_c) of the 40 nm $CoFe_2O_4$ particles is found to be as high as 4.65 kOe.
 [DOI: 10.1063/1.1616655]

The presence of a large magnetocrystalline anisotropy with a reasonable magnetization value makes $CoFe_2O_4$ as promising hard magnetic and recording materials, provided they can be obtained in a stable single domain particle state.[1] However, for nanometer sized $CoFe_2O_4$ particles, the room temperature (RT) coercivity values are reported to be 500–2000 Oe, far below the theoretically estimated one.[2] The observed wide range of coercivities could be related to the difference in the composition and grain size of the samples investigated. In order to obtain a large diameter of the particles, and hence, high coercivity, $CoFe_2O_4$ particles are grown by annealing at high temperatures. This process induces particle growth beyond the single-domain size limit, and consequently, lowers the coercivity. Since it is very difficult to produce $CoFe_2O_4$ particles with narrow size distribution, the estimation of single-domain size of $CoFe_2O_4$ particle has not been discussed for more than four decades since the work of Berkowitz and Scheule.[3] They synthesized stoichiometric cobalt ferrite with different average grain sizes by a low temperature treatment ($<800\,^\circ$C) of coprecipitated metal oxalates. And, the critical size of a single-domain particle of $CoFe_2O_4$ at RT has been claimed to be 70 nm, simply based on the coercivity measurements.[3] Since a mixture of superparamagnetic and single-domain particles would influence the coercivity values,[4] any estimate of the critical single-domain size in their study could be only an approximate one. Therefore, the aim of the present work is to produce nearly monodispersed $CoFe_2O_4$ nanoparticles between 8 and 100 nm directly without any postannealing steps and to determine the single-domain size based on the coercivity and the switching field H_p data, obtained by torque analysis. The authors have proposed seed-mediated growth dominant coprecipitation[5] and modified oxidation[6] methods to synthesize particles with diameters in the ranges 8–40 and 70–100 nm, respectively. In the seed-mediated growth dominant coprecipitation method, various weight fractions of the coprecipitated colloidal $CoFe_2O_4$ were used as seeds to produce particles with diameters as large as 40 nm. At RT a maximum coercivity (H_c) of 2.91 kOe was obtained for the sample synthesized with a seed concentration of 3.33 g/l. Since the seeded $CoFe_2O_4$ has the mixtures of superparamagnetic and single-domain sized particles, size selection[7] was carried out and nearly monodispersed particles of 8, 20, and 40 nm in diameter were produced. In the modified oxidation method, the initial concentration of the ferric ions in the ferrous and ferric ion mixture was controlled and nearly monodispersed particles of about 70 and 100 nm were obtained.

X-ray diffraction (XRD) analyses of the synthesized $CoFe_2O_4$ powders were carried out in a RIGAKU x-ray diffractometer using Cu $K\alpha$ radiation. The particle morphology was examined by using a scanning electron microscope (SEM, Hitachi S-4100) and a high-resolution transmission electron microscope (HRTEM, Hitachi HF-2000). Hysteresis loops were measured using a superconducting quantum interference device magnetometer under a maximum applied field of 50 kOe. The rotational hysteresis loss was evaluated at RT using a torque magnetometer under a maximum applied field of 25 kOe. The ^{57}Fe Mössbauer experiments were performed for the 100, 70, 40, and 20 nm particles of $CoFe_2O_4$ in a Wiessel Mössbauer spectrometer with a 25 mCi ^{57}Co/Rh source kept at RT. The spectrometer was calibrated with a natural iron foil before and after the measurements.

[a]Electronic mail: jeya@mail.kankyo.tohoku.ac.jp

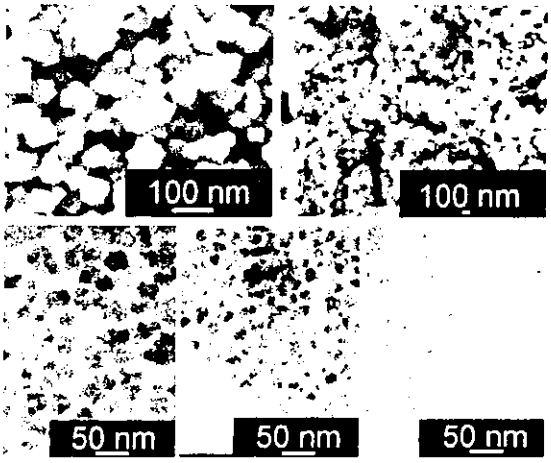

FIG. 1. SEM and TEM micrographs of nearly monodispersed $CoFe_2O_4$ nanoparticles: (a) 100 nm, (b) 70 nm, (c) 40 nm, (d) 20 nm, and (e) 8 nm.

The XRD analysis of all the samples showed the presence of spinel $CoFe_2O_4$ phase only. The SEM and transmission electron microscopy (TEM) micrographs in Fig. 1 show the degree of monodispersity of the particles of sizes between 8 and 100 nm.

Mössbauer spectroscopy measurements were carried out for cobalt ferrite particles of various sizes to determine the cation distribution in the spinel structure. The RT Mössbauer spectra for samples of particle sizes 100, 70, 40, and 20 nm are shown in Figs. 2(a)–2(d). In Figs. 2(a)–2(d), the dots represent the experimental data and the continuous curve is as a result of the least-squares fitting of the data using the Bent program.[8] The Mössbauer spectra have been fitted with three sextets, one corresponding to Fe^{3+} ions in tetrahedral (A) sites and the other two corresponding to Fe^{3+} ions in octahedral (B) site with two different average nearest-neighbor environments. A superparamagnetic doublet was not observed for all the samples except for the sample of 70 nm particle size with a small relative intensity of 6%. The values of the center shifts are characteristic of Fe^{3+} ions. From the relative intensities of the sextets the cation distribution has been arrived at as $(Co_{0.25}Fe_{0.75})[Co_{0.75}Fe_{1.25}]O_4$

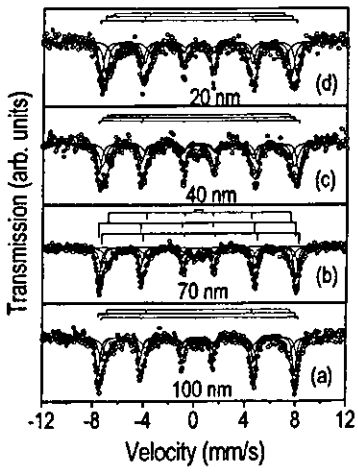

FIG. 2. Room temperature Mössbauer spectra for the nearly monodispersed $CoFe_2O_4$ nanoparticles of various sizes.

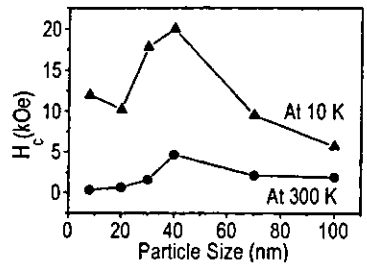

FIG. 3. Coercivity vs particle size of $CoFe_2O_4$ measured at 300 and 5 K in an applied field up to 50 kOe.

for all the samples and the ratio of the population of Fe^{3+} ions in A to B sites is 0.60, which is close to the value of 0.67 obtained by Moumen *et al.* for their 5 nm size particles.[9] The weighted average hyperfine field for the 100, 70, and 40 nm samples was 480 kOe, whereas for the 40 nm particle it was 450 kOe, only due to a large fraction of surface spins with smaller magnetic moments.

Figure 3 shows the variation of coercivity as a function of particle size at RT and 10 K. The coercivity increases with particle size and reaches a maximum of 4.65 kOe at RT for the 40 nm particle size, and thereafter it decreases with any further increase in particle size. At 10 K, the coercivity is higher compared to the values at RT for a given particle size. This can be due to the increase in magnetocrystalline anisotropy at low temperatures.[10] It could be noted that the H_c of 4.65 kOe for the 40 nm $CoFe_2O_4$ particles at RT is the highest and also close to the theoretical value of 5.3 kOe. The value of squareness ratio (M_r/M_s) of 0.66 indicates that the system consists of randomly oriented equiaxial particles with cubic magnetocrystalline anisotropy.[11] The particle size dependent coercivity studies reveal that the single-domain size of the $CoFe_2O_4$ is about 40 nm.

To confirm the single-domain size limit of $CoFe_2O_4$, rotational hysteresis loss analysis using a torque magnetometer was performed. The inset of Fig. 4 shows the representative magnetic field dependence of the rotational hysteresis loss (W_r) for the 40 nm $CoFe_2O_4$ particles. With increasing field, W_r gradually increases and shows a peak at 17 kOe. The peak corresponds to the average switching field H_p, the

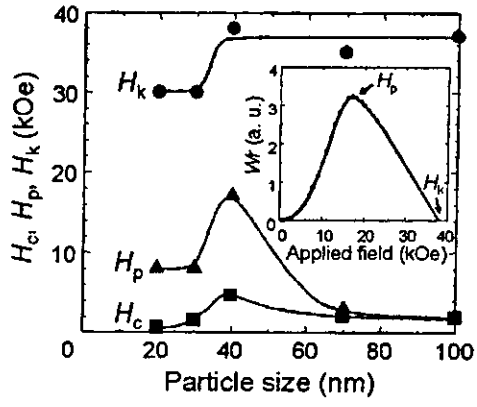

FIG. 4. Room temperature coercivity H_c, peak field H_p, and magnetic anisotropy field H_k vs particle diameter of the $CoFe_2O_4$ nanoparticles. The inset shows the plot of rotational hysteresis loss W_r vs applied magnetic field H for 40-nm-sized $CoFe_2O_4$ particles (continuous line is a guide for the eye).

field at which irreversible magnetization reversal occurs. With a further increase of the magnetic field, W_r gradually decreases. It is to be noted that W_r still does not vanish even at a high applied field of 25 kOe. The magnetic anisotropy field H_k is determined[12,13] at $W_r=0$ by extrapolating the linear part of W_r, and it is 38 ± 1 kOe. The magnetocrystalline anisotropy $K(K=M_sH_k/2$; where $M_s=53$ emu/g at RT for the 40 nm particles) is estimated to be about 5.1×10^6 ergs/cc, and is in good agreement with the value of the bulk $CoFe_2O_4$.[10]

Figure 4 shows the anisotropy field H_k and the switching field H_p of $CoFe_2O_4$ particles plotted against the particle size in the range 20–100 nm. For comparison, H_c at RT is also shown in Fig. 4. Both H_k and H_p show a maximum at 40 nm and they are very small for smaller particle sizes. H_p shows a smaller value of about 2–3 kOe for the 70 and 100 nm particles. It is found that H_p is much larger than H_c for the particles in the 20–40 nm particle size regime, while H_p is comparable to H_c for the 70–100 nm particle sizes. Numerical analysis of an assembly of single-domain particles, whose easy axes of magnetization are three-dimensionally oriented, shows that H_p will be larger than H_c provided that the magnetic exchange interaction between particles is low.[11] Since the δM plot[14] of the nearly monodispersed 40 nm particle shows a negative maximum, we can say that the magnetic exchange interaction between the particles is negligible. Therefore, the fact that H_p is much larger than H_c for the particles in the 20–40 nm size regime implies that the particles are in the single-domain state. On the other hand, the H_p values, which are comparable to H_c for the 70–100 nm particles, can be explained only if we assume that the magnetization reversal mechanism of the particles is dominated by domain wall motion, i.e., the particles are in the multidomain state. Thus, the H_c and H_p studies suggest that the critical size of the single-domain $CoFe_2O_4$ particles is about 40 nm and not 70 nm as reported by Berkowitz and Schuele.[2]

In conclusion, $CoFe_2O_4$ nanoparticles with average sizes between 8 and 100 nm were synthesized using the seed-mediated coprecipitation method followed by size separation and also the oxidation method. Particles synthesized by these methods were confirmed to have a similar cation distribution of $(Co_{0.25}Fe_{0.75})[Co_{0.75}Fe_{1.25}]$ from Mössbauer spectroscopy analysis. The RT magnetic anisotropy field H_k and magnetocrystalline anisotropy K values were 38 kOe and 5.1×10^6 erg/cc, respectively. The $CoFe_2O_4$ particles of about 40 nm in size exhibited a coercivity value of 4.65 kOe and a squareness ratio (M_r/M_s) of 0.66 at 300 K. Both the switching field H_p, obtained by the magnetic torque analysis, and the coercive field H_c suggested that the critical size of single-domain $CoFe_2O_4$ particles was 40 nm.

[1] S. Chikazumi, *Physics of Magnetism* (Wiley, New York, 1969), p. 100.
[2] M. Grigorova, H. J. Blythe, V. Blaskov, V. Rusanov, V. Petkov, V. Masheva, D. Nihtianova, L. M. Martinez, J. S. Muñoz, and M. Mikhov, J. Magn. Magn. Mater. **183**, 163 (1998).
[3] A. E. Berkowitz and W. J. Schuele, J. Appl. Phys. **30**, 134S (1959).
[4] C. P. Bean, J. Appl. Phys. **26**, 1381 (1955).
[5] C. N. Chinnasamy, B. Jeyadevan, O. Perales-Perez, K. Shinoda, K. Tohji, and A. Kasuya, IEEE Trans. Magn. **38**, 2640 (2002).
[6] C. N. Chinnasamy, M. Senoue, B. Jeyadevan, Oscar Perales-Perez, K. Shinoda, and K. Tohji, J. Colloid Interface Sci. **263**, 80 (2003).
[7] O. Perales-Perez, H. Sasaki, A. Kasuya, B. Jeyadevan, K. Tohji, T. Hihara, and K. Sumiyama, J. Appl. Phys. **91**, 6958 (2002).
[8] M. F. Bent, P. Persson, and D. G. Agresti, Comput. Phys. Commun. **1**, 67 (1969).
[9] N. Moumen, P. Bonville, and M. P. Pileni, J. Phys. Chem. **100**, 14410 (1996).
[10] R. M. Bozorth, E. F. Tilden, and A. J. Williams, Phys. Rev. **99**, 1788 (1955).
[11] A. E. Berkowitz and E. Kneller, *Magnetism and Metallurgy* (Academic, New York, 1969), Vol.1, Chap.8.
[12] M. Takahashi, T. Shimatsu, M. Suekane, M. Miyamura, K. Yamaguchi, and H. Yamasaki, IEEE Trans. Magn. **28**, 3285 (1992).
[13] I. S. Jacobs and F. E. Luborsky, J. Appl. Phys. **28**, 467 (1957).
[14] C. N. Chinnasamy, B. Jeyadevan, D. J. Djayaprawira, K. Tohji, and M. Takahashi (unpublished).

Ultra-stable nanoparticles of CdSe revealed from mass spectrometry

ATSUO KASUYA*[1], RAJARATNAM SIVAMOHAN[1], YURII A. BARNAKOV[1], IGOR M. DMITRUK[1], TAKASHI NIRASAWA[2,3], VOLODYMYR R. ROMANYUK[1], VIJAY KUMAR[1,4,5], SERGIY V. MAMYKIN[1], KAZUYUKI TOHJI[2], BALACHANDRAN JEYADEVAN[2], KOZO SHINODA[2], TOSHIJI KUDO[3], OSAMU TERASAKI[6], ZHENG LIU[6], RODION V. BELOSLUDOV[4], VIJAYARAGHAVAN SUNDARARAJAN[1,7] AND YOSHIYUKI KAWAZOE[4]

[1]Center for Interdisciplinary Research, Tohoku University, Sendai, 980-8578, Japan
[2]Graduate School of Environmental Studies, Tohoku University, Sendai, 980-8579, Japan
[3]Bruker Daltonics K.K., Kanagawa-ku, Yokohama, 221-0022, Japan
[4]Institute for Materials Research, Tohoku University, Sendai, 980-8577, Japan
[5]Dr Vijay Kumar Foundation, Chennai, 600 078, India
[6]Department of Physics, Tohoku University, Sendai, 980-8578, Japan
[7]Centre for Development of Advanced Computing, Pune, 411 007, India
*e-mail: kasuya@cir.tohoku.ac.jp

Published online: 25 January 2004; doi:10.1038/nmat1056

Nanoparticles under a few nanometres in size have structures and material functions that differ from the bulk because of their distinct geometrical shapes and strong quantum confinement. These qualities could lead to unique device applications. Our mass spectral analysis of CdSe nanoparticles reveals that $(CdSe)_{33}$ and $(CdSe)_{34}$ are extremely stable: with a simple solution method, they grow in preference to any other chemical compositions to produce macroscopic quantities. First-principles calculations predict that these are puckered $(CdSe)_{28}$-cages, with four- and six-membered rings based on the highly symmetric octahedral analogues of fullerenes, accommodating either $(CdSe)_5$ or $(CdSe)_6$ inside to form a three-dimensional network with essentially heteropolar sp^3-bonding. This is in accordance with our X-ray and optical analyses. We have found similar mass spectra and atomic structures in CdS, CdTe, ZnS and ZnSe, demonstrating that mass-specified and macroscopically produced nanoparticles, which have been practically limited so far to elemental carbon[1], can now be extended to a vast variety of compound systems.

Single-sized, stable nanoparticles are highly valuable because they have well-defined structures that can be identified with atomic precision. Their specific physical and chemical properties can be analysed, or realised, on the basis of their particular atomic arrangements. Such assemblies of atoms may serve as versatile building blocks for functional materials in nanometre science and technology. Recent extensive studies show that they could be produced not just in carbon but in other elements and compounds that may have electronic, optical and medical applications: examples are metal-encapsulated Si clusters[2], polyhedral-shell-like BN[3,4], and size- or shape-controlled II–VI compounds[5–7]. Here we report the synthesis and identification of mass-selected $(CdSe)_{33}$ and $(CdSe)_{34}$ nanoparticles in solution. These constitute the first compound nanoparticles that are stable and macroscopically produced at precisely specified numbers of constituent atoms with their stoichiometric composition identical to the bulk solids.

$(CdSe)_n$ nanoparticles were prepared in reverse micelles (see Methods). The sample in toluene was dried on the target plate of a time-of-flight mass spectrometer equipped with a nitrogen laser. Curve 1 in Fig. 1 shows the mass spectrum of positive ions from this sample produced by laser vaporization without cooling by carrier gas injection in the vacuum chamber. It shows three dominant peaks at $n = 13, 33$ and 34 with 1:1 stoichiometry of Cd/Se as in the bulk, together with much weaker peaks for off-stoichiometric particles. The peak width represents binomial isotope distributions of naturally abundant Cd and Se atoms. The intensities of the peaks at 33 and below tend to increase relative to 34 as the laser power increases, indicating that particles of $n < 33$ may also be produced by fragmentation of 33 and 34. The characteristic feature of curve 1 is that only the two peaks at $n = 33$ and 34 appear prominently in a region of the plot that covers a very wide range of mass (more than 19 CdSe units), indicating that only $(CdSe)_{33}$ and $(CdSe)_{34}$ are grown in the solution because of their extremely selective stabilities. From atomic force microscopy (AFM) measurement of the step height on a few-monolayer film deposited on graphite, we determined the diameter of these nanoparticles to be 1.5 nm.

To see the stability of these nanoparticles further, we measured mass spectra from laser ablation of bulk crystalline samples of CdSe, CdS, ZnS and ZnSe. They all show appreciable peaks at $n = 13, 33$ and 34, which are produced even in the violent ablation process, which would be expected to fragment the clusters into lower-mass particles. This indicates the extreme stability of particles at $n = 33$ and 34 without ligands as noted in

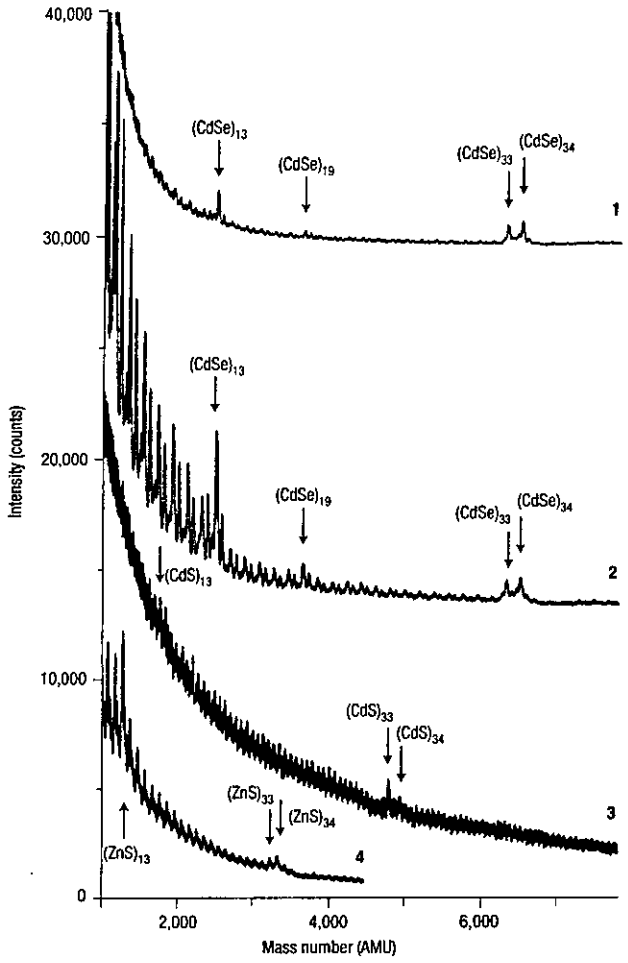

Figure 1 Time-of-flight mass spectra of positive ions. Curve 1 is for nanoparticles of CdSe prepared in toluene. Other mass spectra are produced by laser ablation of bulk powders of CdSe (curve 2), CdS (curve 3) and ZnS (curve 4).

curves 2, 3 and 4 of Fig. 1, which show CdSe, CdS and ZnS, respectively. Martin[8] finds a similar tendency for ZnS with helium gas cooling during ablation.

Measurements of optical absorption in solution give additional evidence that our sample contains stable mass-selected nanoparticles. Curve 1 of Fig. 2 has a sharp excitonic peak at 415 nm together with smaller peaks at 382 nm and 352 nm, blueshifted considerably from the bulk value of 680 nm. This indicates that the solution contains only specific sizes of nanoparticles. These three peaks are reproducible, not only in spectral positions, but also in the relative intensity ratios in each sample measured. The blueshifted peak at 415 nm for our nanoparticles of diameter 1.5 nm is also consistent with the value of energy estimated from the size-dependent spectra of Murray *et al.*[5]. The main component of our sample in toluene, therefore, is identified as only $(CdSe)_{33}$ and $(CdSe)_{34}$. The spectral profile of curve 1 is practically identical to those reported by Murray *et al.*[5] and Ptatschek *et al.*[6], who estimated the diameters of the nanoparticles to be 1.2 nm and 1.7 nm, respectively. These results show that these nanoparticles are especially stable, as they will grow under a wide range of preparation conditions.

Curve 2 of Fig. 2 shows the absorption spectrum of the solution prepared at 80 °C. A new broad peak appears at 480 nm, indicating that

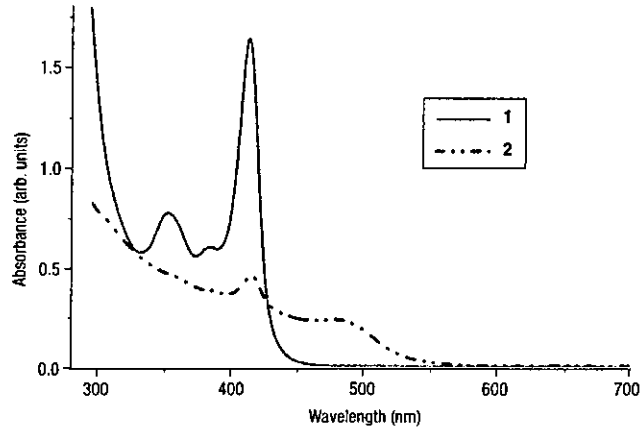

Figure 2 Optical absorption spectra at room temperature. Curve 1 is for CdSe nanoparticles prepared in toluene at 45 °C. Curve 2 is for a sample prepared at 80 °C, showing a new broad peak at 480 nm, with the sharp peak at 415 nm in curve 1 remaining without shift. At higher temperatures and longer times, the broad peak redshifts and its intensity increases, whereas the sharp peak decreases without shift.

particles of a new type begin to grow with a mean diameter of 2.0 nm and a distribution of ~10%, which is typical of small crystalline-like particles prepared with conventional colloid methods[5,6]. This broad peak shifts to longer wavelength with increasing temperature and time as the particle size increases. The sharp peak at 415 nm in curve 1 remains in curve 2 without shift, showing that $(CdSe)_{33}$ and $(CdSe)_{34}$ have particularly stable structures that are highly resistant against ripening even under conditions that favour the growth of larger particles.

Figure 3 shows X-ray diffraction profiles on our sample dried in air after removing the excess surfactant (curve 1), and on a powder sample of crystalline CdSe (curve 2). Curve 1 shows a series of five clear peaks indicated by arrows below $2\theta = 15°$. The first peak, at 2.80°, is the

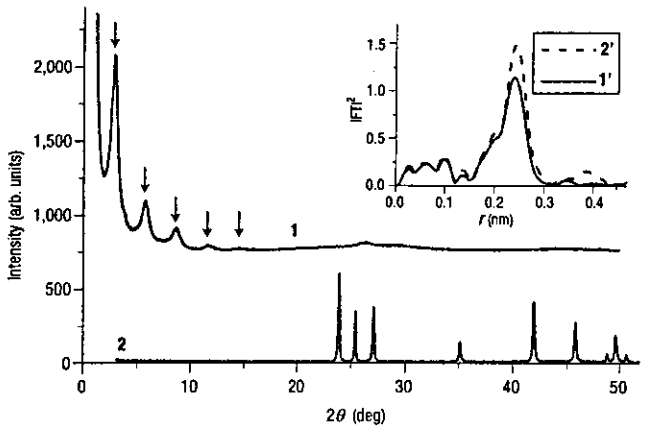

Figure 3 X-ray analysis of $(CdSe)_{33}$ and $(CdSe)_{34}$ structures. Curve 1 is the X-ray diffraction profile of a dried sample containing $(CdSe)_{33}$ and $(CdSe)_{34}$, taken with Cu-Kα radiation, and curve 2 is for a powder of bulk wurtzite CdSe. The curves 1′ and 2′ in the inset show the Fourier transform of EXAFS spectra at the Se-K edge of the nanoparticle and powder samples, respectively. *r*: nearest-neighbour distance.

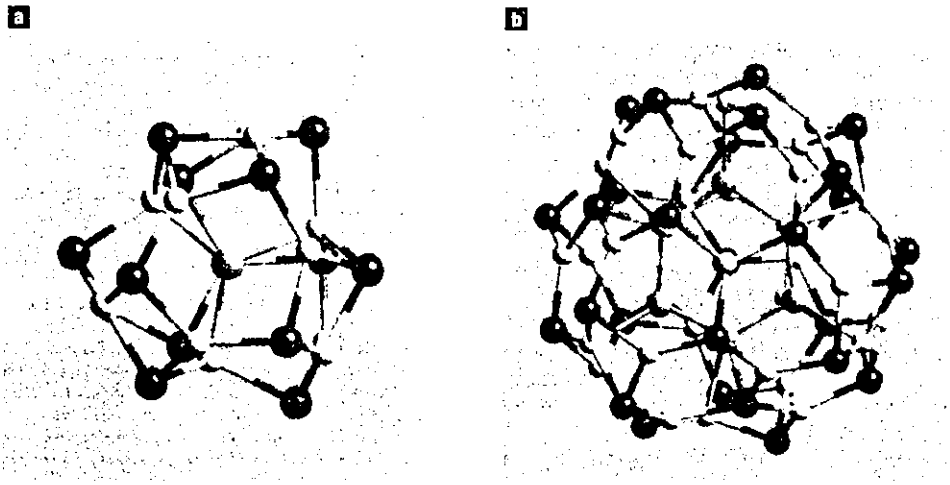

Figure 4 Structures of the $(CdSe)_n$ core–cage nanoparticles calculated to be most stable, viewed down a threefold symmetry axis. a, $(CdSe)_{13}$ has 3 four-membered and 10 six-membered rings on the cage of 12 Se (dark brown) and 13 Cd (white) ions with a Se (light brown) ion inside. **b**, $(CdSe)_{34}$ has a truncated-octahedral morphology formed by a $(CdSe)_{28}$-cage (Se, dark brown; Cd, white) with 6 four-membered and 8 × 3 six-membered rings. A $(CdSe)_6$ cluster (Se, light brown; Cd, green) encapsulated inside this cage provides additional network and stability.

fundamental reflection of the next four higher-order ones. These low-angle reflections show a self-assembled stack constructed from $(CdSe)_{33}$ and $(CdSe)_{34}$ with the surfactant acting as a spacer. Our wet chemical analysis and energy-dispersive X-ray (EDX) measurement of the solid sample show 1:1 stoichiometry of Cd/Se.

At angles of $2\theta > 20°$ there are only weak features in curve 1 where crystalline peaks of the bulk wurtzite CdSe would appear (curve 2). The width and shift of these weak features indicate that the range of structural ordering is ~1 nm in the arrays. EXAFS (extended X-ray absorption fine structure) measurement on $(CdSe)_{33}$ and $(CdSe)_{34}$ in toluene (Fig. 3, inset) shows a clear Fourier transform peak for a nearest-neighbour atom distance of 0.260 nm compared with 0.263 nm for bulk CdSe with tetrahedral bonding. The coordination number of Se ions is estimated to be 3.2 as compared with 4 in the bulk and 3 in the empty cage structure of, for example, C_{60} and $(BN)_n$. Peaks for further neighbours are weaker and much spread around the bulk second neighbour peak at 0.40 nm. These results show that our nanoparticles have basically three-dimensional sp^3-bonded Cd–Se with the modifications expected in particles of less than 100 atoms[9], consistent with our theoretical analysis given below.

First-principles calculations using ultrasoft pseudopotentials and the generalized gradient approximation[10] show $(CdSe)_n$ to be cage-like polyhedra with sp^3-like zigzag networks of alternately connected Cd and Se ions forming four- and six-membered rings similar to $(BN)_n$ (ref. 3) but highly puckered. Further stabilization occurs by filling the cage with a core connected to the cage. The choice of a highly symmetric cage with the right size of core imposes stringent restrictions for the stable nanoparticles if they are to retain a tetrahedral-like 3D network internally. This novel 3D core–cage structure shows magic behaviour (certain 'magic numbers' are strongly favoured) entirely different from fullerenes[1,2], BN-cages[3,4], shell structures of metallic clusters[8] and bulk fragments of compound nanoparticles[5–7]. The smallest polar cages with the highest possible symmetry (octahedral) are for $n = 12$, 16 and 28. Cages with $n = 12$ and 28 can accommodate, respectively, $(CdSe)_1$ and $(CdSe)_6$ inside as just the right sizes to form basically tetrahedral networks, making up stable $(CdSe)_{13}$ and $(CdSe)_{34}$ (Fig. 4) after rearranging their structures to maximize the binding energy. For $(CdSe)_{33}$, $(CdSe)_5$ fits well into the $(CdSe)_{28}$-cage, keeping a similar network. The encapsulation of $(CdSe)_3$ into an $n = 16$ cage is unfavourable as the inner space is too small. The optimal structure of $(CdSe)_{19}$ is a low-symmetry $n = 18$ cage encapsulating $(CdSe)_1$ with a local maximum in the binding energy leading to its weak magic nature (Fig. 1).

$(CdSe)_{13}$ has 12 Se and 13 Cd ions making up the puckered cage and a Se ion at the centre connected with four Cd ions 0.282 nm apart (Fig. 4a). The mean Cd–Se bond length is 0.264 nm. It is 0.614 eV lower in energy than an empty $n = 13$ cage, showing the preference for a 3D network. Fragments of bulk wurtzite and zinc blende[8] structures transform significantly on relaxation and lie a few electron volts higher

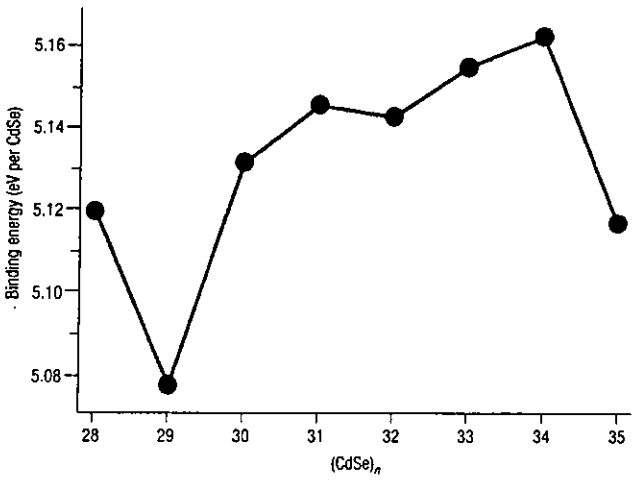

Figure 5 Calculated binding energies. The binding energies are calculated per CdSe molecule of $(CdSe)_n$ composed of a cage-like $(CdSe)_{28}$ with $(CdSe)_m$ inside ($n = 28 + m$, $m = 0, 1, \ldots, 7$).

in energy than the core–cage structures, ruling out the possibility that $(CdSe)_{13}$ and $(CdSe)_{34}$ have the bulk structure. The bond lengths in $(CdSe)_{34}$ (Fig. 4b) vary from 0.255 to 0.284 nm with the mean value of 0.266 nm, as compared with 0.268 nm calculated for the bulk. The mean nearest-neighbour coordination is 3.18. These results agree well with our EXAFS analysis. The largest diameter (1.45 nm) of $(CdSe)_{34}$ also agrees with our AFM estimate of 1.5 nm as well as the previous[5,6] estimates. The binding energy is maximum for $(CdSe)_{34}$ among $(CdSe)_{28+m}$ with $m = 0, 1, \ldots, 7$, as $(CdSe)_{m=6}$ is just the right size to fit inside a $(CdSe)_{28}$-cage, resulting in its extreme stability (Fig. 5). The binding energy decreases only slightly for $(CdSe)_{33}$ with $m = 5$. Our calculations also predict such nested cages with a core for other II–VI compounds, for example, ZnS and CdS, again supporting our experimental results. However, core–cage structures are less stable for III–V nanoparticles. For example, $(BN)_{13}$ with N at the centre is less stable than the empty $(BN)_{12}$ and $(BN)_{13}$-cages[3].

Our investigations demonstrate that $(CdSe)_n$ are extremely stable at some specific n, with novel core–cage structures predicted by theory. This sharply selective stability provides a definitive identification of stable compound nanoparticles of particular atomic numbers and compositions. Such 'magic clusters'[6] have long been sought or proposed on the basis of experiments. Our methods should allow their production in macroscopic quantities.

METHODS

PREPARATION

$(CdSe)_n$ nanoparticles were prepared in reverse micelles at a temperature of 45 °C under ambient pressure. Cadmium nitrilotriacetate, obtained by dissolving 0.16 g of $CdSO_4$ and 0.21 g of sodium nitrilotriacetic acid in 10 ml of water, was mixed with 1.2 ml of decylamine ($CH_3(CH_2)_4NH_2$) as surfactant. The cadmium ions bind to the amine groups of the surfactant. The solution is further mixed with 15 ml aqueous solution of sodium selenosulphate (Na_2SeSO_3) which dissociates in alkaline conditions to yield Se^{2-}. On adding toluene to this solution, the micelles move up into the toluene and transform into reverse micelles in which nanoparticles of CdSe form. Within a few minutes the toluene turns uniformly to greenish yellow, whereas the water remains colourless. The total reaction yield is more than 20%.

MASS SPECTROMETRY

The time-of-flight mass spectrometer used was a Bruker Daltonics, Reflex III, equipped with a nitrogen laser.

Received 8 July 2003; accepted 10 December 2003; published 25 January 2004.

References

1. Kraetschmer, W., Lamb, L. D., Fostiropoulos, K. & Huffman, D. R. Solid C_{60}: A new form of carbon. *Nature* 347, 27–30 (1990).
2. Kumar, V. & Kawazoe, Y. Metal-encapsulated fullerene like and cubic caged clusters of silicon. *Phys. Rev. Lett.* 87, 045503 (2001).
3. Seifert, G., Fowler, P. W., Mitchell, D., Porezag, D. & Frauenheim, Th. Boron-nitrogen analogues of the fullerenes: Electronic and structural properties. *Chem. Phys. Lett.* 268, 352–358 (1997).
4. Stephan, O. *et al.* Formation of small single-layer and nested BN cages under electron irradiation of nanotubes and bulk material. *Appl. Phys. A* 67, 107–111 (1998).
5. Murray, C. B., Norris, D. J. & Bawendi, M. G. Synthesis and characterization of nearly monodisperse CdE (E = S, Se, Te) semiconductor nanocrystallites. *J. Am. Chem. Soc.* 115, 8706–8715 (1993).
6. Ptatschek V. *et al.* Quantized aggregation phenomena in II–VI semiconductor colloids. *Ber. Bunsenges. Phys. Chem.* 102, 85–95 (1998).
7. Peng, X. *et al.* Shape control of CdSe nanocrystals. *Nature* 404, 59–61 (2000).
8. Martin, T. P. Shells of atoms. *Phys. Rep.* 273, 199–241 (1996).
9. Pinto, A. *et al.* Evidence for truncated octahedral clusters in supported gold clusters. *Phys. Rev. B* 51, 5315–5321 (1995).
10. Kresse, G. & Furthmuller, J. Efficient iterative schemes for ab-initio total energy calculations using a plane-wave basis set. *Phys. Rev. B* 55, 11169–11186 (1996).

Acknowledgements

The authors are indebted to M.Tachiki, Y.Nishina, K.Suzuki, A.Inoue, K.Sumiyama, T.Ohsuna and J. R. Anderson for discussions and comments.

Correspondence and requests for materials should be addressed to A.K.

Supplementary Information accompanies the paper on www.nature.com/naturematerials

Competing financial interests

The authors declare that they have no competing financial interests.

Available online at www.sciencedirect.com
SCIENCE DIRECT®
Chemical Physics Letters 385 (2004) 323–328
CHEMICAL PHYSICS LETTERS
www.elsevier.com/locate/cplett

Electronic properties of radial single-walled carbon nanotubes

Yoshinori Sato [a,*], Balachandran Jeyadevan [b], Rikizo Hatakeyama [a], Atsuo Kasuya [c], Kazuyuki Tohji [b]

[a] Graduate School of Engineering, Tohoku University, Aoba 05 Aramaki Aoba-ku, Sendai 980-8579, Japan
[b] Graduate School of Environmental Studies, Tohoku University, Sendai 980-8579, Japan
[c] Center for Interdisciplinary Research, Tohoku University, Sendai 980-8578, Japan

Received 15 December 2003; in final form 15 December 2003
Published online: 22 January 2004

Abstract

We investigated the electronic properties of the radial single-walled carbon nanotubes (SWCNTs) by using the Raman and the UV–Vis–NIR spectroscopy. The radial SWCNTs for the analysis were synthesized by the arc-discharge method with Ce as a catalyst. The yield of the radial SWCNTs with 1.55 nm diameter and 60 nm length was as high as 20% in the soot. From the UV–Vis–NIR spectrum and the tangential mode of Raman spectra, the radial SWCNTs were confirmed to be composed of semiconducting (0.64 and 1.14 eV for $V_s^1 \rightarrow C_s^1$ and $V_s^2 \rightarrow C_s^2$) and metallic (1.60 eV for $V_m^1 \rightarrow C_m^1$) nanotubes.

1. Introduction

The discovery [1,2], high-yield synthesis [3] and purification [4,5] of single-walled carbon nanotubes (SWCNTs) with novel properties have inspired scientists from various disciplines working on a range of potential applications [6–9]. Physical [10], chemical [11] and mechanical [12] properties of SWCNTs depend on their diameter, chirality and morphology. In the SWCNTs, there are two type morphologies; one is a tens of micrometer long SWCNTs, the so-called 'highway junction type SWCNTs' and the other is a tens of nanometer long radial SWCNTs, often referred to as 'sea urchin type SWCNTs'. Highway junction type SWCNTs have been synthesized by means of the arc-discharge method or the laser vaporization method using the bi-metal catalyst, Ni/Co, Ni/Fe, Ni/Y and Rh/Pd. Also, the optical properties of the highway junction type SWCNTs have been studied in detail and have been found to be composed of both semiconducting and metallic tubes [13,14]. On the other hand, radial SWCNTs with 1.5–2.0 nm in diameter and 50–100 nm in length are grown radially around the core metal particles. They have been synthesized by an arc-discharge [15–17] and solar focused production method [18] using a metal catalyst such as, Y, La, Ce and Gd. However, the production efficiency of the radial SWCNTs has been reported to be very low (roughly 6% by volume from visual inspection of TEM images [19]) and no detailed study has been carried out to improve the production efficiency. As a result, there is little or no information about their electronic properties [18,20]. Alvarez et al. [18,20] have synthesized the radial SWCNTs by the solar focused production method using La as a catalyst. They measured the Raman spectra of radial SWCNTs with diameters from 1.5 to 1.8 nm using the incident light energy of 1.92, 2.41 and 2.54 eV and reported that the tube possesses semiconducting character due to no Breit–Wigner–Fano (BWF) lineshape resonance. However, in order to investigate the metallic nature of these nanotubes, Raman spectroscopic measurement with laser energy close to 1.5 eV will be necessary and the electronic structure of the radial SWCNTs is yet to be clarified. Here, we discuss the parameters that need to be optimized for efficient production of radial SWCNTs by using the arc-discharge method with Ce as a catalyst. And also, we report their electronic structure by using Raman and UV–Vis–NIR spectroscopy.

* Corresponding author. Fax: +81-22-217-7391.
E-mail address: hige@bucky1.kankyo.tohoku.ac.jp (Y. Sato).

0009-2614/$ - see front matter © 2004 Elsevier B.V. All rights reserved.
doi:10.1016/j.cplett.2004.01.004

2. Experimental

Radial SWCNTs were synthesized by a direct current arc-discharge between a pure graphite cathode and a metal loaded graphite anode in helium atmosphere. A 16 mm diameter and 50 mm long pure graphite rod (purity 99.9%) and a 6 mm diameter and 85 mm long graphite rod (99.9%) loaded with CeO_2 powder (99.99%) as the source of Ce metal were used as cathode and anode, respectively. The soot samples were synthesized by varying the He gas (99.99%) pressure from 100 to 1500 Torr and the arc-discharge current from 60 to 100 A. The sample for the investigation was collected only from the inner wall of the chamber and burned in air at 533 K for 1 h to remove the amorphous carbon. Transmission electron microscope (TEM) (Hitachi HF-2000) with a field emission type electron gun was used to observe the morphology of the soot. Raman spectrometers, Jobin-Yvon T64000 with Ar ion (Leonix Co.) and He-Ne (NEC Co.) lasers and Jobin-Yvon LabRam HR-800 with diode laser (TOPTICA Photonics AG.), were used to analyze the physical properties of radial SWCNTs. Samples were measured using 488.0, 514.5, 632.8 and 785.0 nm exciting lasers under backscattering configuration. The UV–Vis–NIR spectrum of the radial SWCNTs thin film was measured with a Hitachi U-4100 spectrophotometer. The used film was prepared by the method described below. First, 10 mg of radial SWCNTs soot was ultrasonicated in 100 mL of butyl acetate to prepare a homogeneous dispersion. Finally, the suspension was sprayed on a quartz plate using an airbrush. Then, the film was dried at 473 K in vacuum (10^{-3} Torr) for 24 h to remove the butyl acetate absorbed on SWCNTs.

3. Results and discussion

Fig. 1a–c show the Raman intensity ratio I_G/I_D of the soot synthesized under a varying He gas pressure, arc current and Ce concentration, respectively. Here, the Raman spectra were measured using the incident light of 2.54 eV. Raman scattering peaks corresponding to E_{2g} vibration modes at 1568 and 1590 cm^{-1} in the tangential mode range were due to the zone folding effect of the SWCNTs. Since the peak at 1350 cm^{-1} is the Raman active mode of the defective carbon network, the intensity is roughly proportional to the amount of amorphous carbon in the sample. Therefore, the Raman intensity ratio I_G/I_D of the peaks at 1350 cm^{-1} (D-band) and 1590 cm^{-1} (G-band) is a good index for the evaluation of SWCNTs abundance. As seen in Fig. 1, the productivity of radial SWCNTs was very sensitive to He pressure and arc current for the soot synthesized with Ce concentration of about 1.7 at.%. In the arc-discharge, the temperature of the arc plasma changes by the gas pressure, arc-discharge current, or convection [21–23]. We suppose that the production of radial SWCNTs is influenced very much by the temperature distribution and its gradient around the arc plasma [24]. Thus, the optimum synthesis condition for a high yield of SWCNTs was found to be Ce concentration of 1.7 at.%, He pressure of 500 Torr and arc-discharge current of 70 A. We characterized the radial SWCNTs synthesized under the above condition.

Fig. 2 shows the typical low magnification TEM images of the soot synthesized under He gas pressures of (a) 100 Torr and (b) 500 Torr, while the Ce concentration in the anode and arc-discharge current were 1.7 at.% and 70 A, respectively. In the soot synthesized under the He pressure of 100 Torr, radial SWCNTs were not produced as seen in Fig. 2a. Also, most of the Ce metal nanoparticles were buried in spherical amorphous carbon particles. On the other hand, large quantities of radial SWCNTs were observed in the soot synthesized at the He pressure of 500 Torr. Fig. 2c is the high-resolution TEM image of the radial SWCNTs soot. From the TEM observation, it is found that the average diameter of SWCNTs was 1.6 nm in the range between 1.4 and 2.1 nm. The length was distributed between 50 and

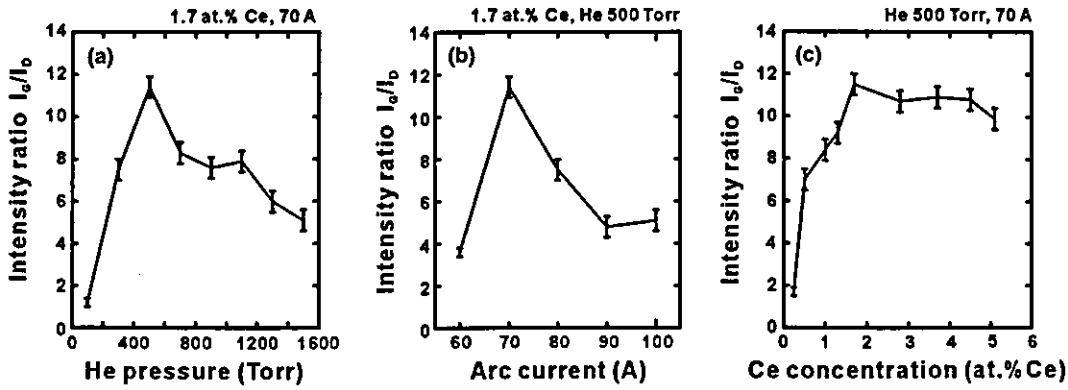

Fig. 1. The Raman intensity ratios I_G/I_D of the soot synthesized under varying: (a) He gas pressure; (b) arc current; (c) Ce concentration. Raman spectra were measured using the incident light of 2.54 eV.

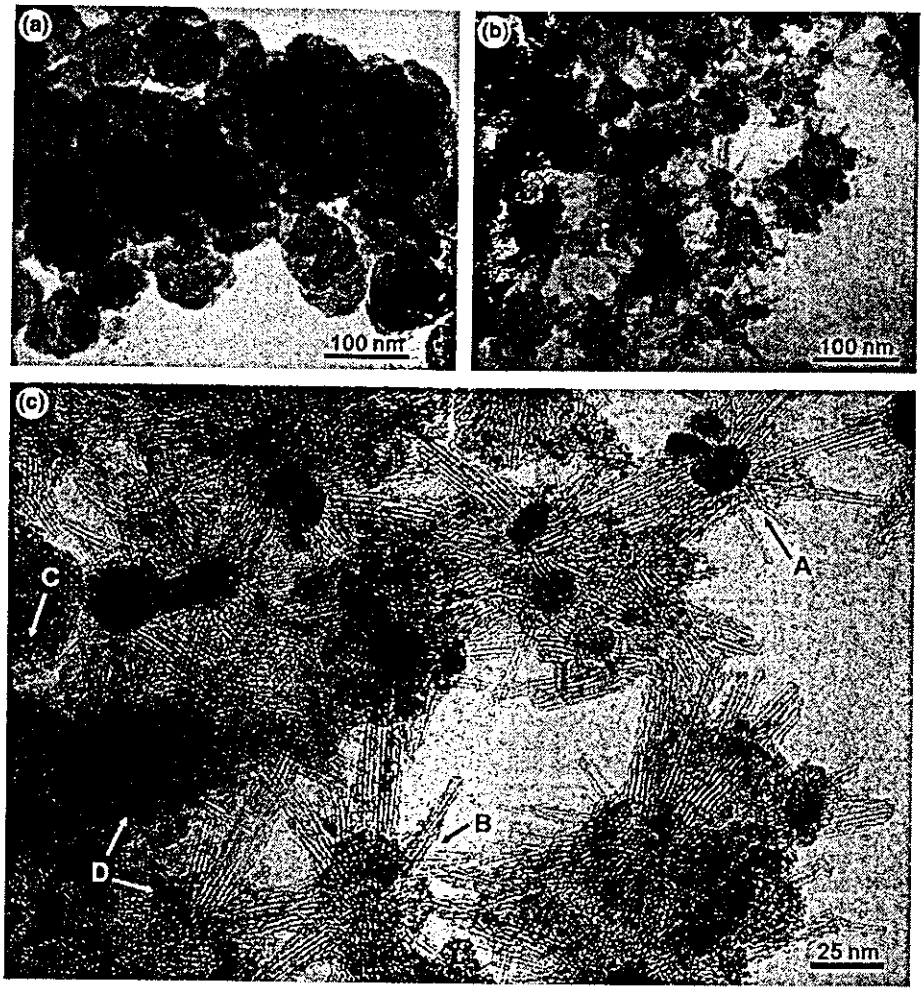

Fig. 2. Typical low magnification TEM images of the soot synthesized under a He gas pressure of (a) 100 Torr (b) 500 Torr while the Ce concentration in the anode and arc-discharge current were 1.7 at.% and 70 A, respectively. (c) A high-resolution TEM image of radial SWCNTs soot synthesized under a He gas pressure of 500 Torr shows (A) radial SWCNTs with Ce carbide metal particle at the core, (B) radial SWCNTs with small metal particles at the core, (C) amorphous carbons and (D) Ce carbide particles.

70 nm and was shorter than that of the highway junction type. The diameter of bundles grown from Ce compound core was not always uniform and but it varied between 5.0 and 16.0 nm. The soot consisted of (arrow A) radial SWCNTs with Ce carbide metal particle at the core, (arrow C) amorphous carbon and (arrow D) Ce carbide particles as shown in Fig. 2c. However, not all of the core metals can be formed in the radial SWCNTs; there are some radial SWCNTs with the aggregated small metal particles around the core as shown in arrow B. The yield of radial SWCNTs was estimated to be about 20% from the TEM observations.

Fig. 3a, b show the radial breathing mode (RBM) and tangential mode (TM) ranges of Raman spectra using exciting laser with various photon energies for the soot synthesized at Ce concentration of 1.7 at.%, He pressure of 500 Torr and arc-discharge current of 70 A and subsequently burned in air at 533 K for 1 h. As shown in Fig. 2, the radial SWCNTs were self-assembled into bundles and the diameter distribution of radial SWCNTs was determined from the Raman line in RBM range using the equation

$$\nu(\mathrm{cm}^{-1}) = 223.5(\mathrm{cm}^{-1}\mathrm{nm})/d(\mathrm{nm}) + 12.5$$

derived from the van der Waals interaction of the nanotube packing [25]. To suppress the resonant Raman effect, an incident light with photon energy of 2.54 eV was used along with 2.41 eV [14]. From the peaks at 149 and 159 cm^{-1}, the mean diameter of the radial SWCNTs was estimated to be about 1.55 nm. These results were in good agreement with the diameter observed from the TEM images. In the profiles obtained by using the incident lights of 1.96, 2.41 and 2.54 eV in the TM range, the peak often observed in graphite at 1580 cm^{-1}, split into two peaks with their peak positions at 1570 and 1590 cm^{-1}. On the other hand, in the Raman spectrum measured using the incident light of 1.57 eV, a strong peak at 1588 cm^{-1} followed by a weak one at 1566 cm^{-1}

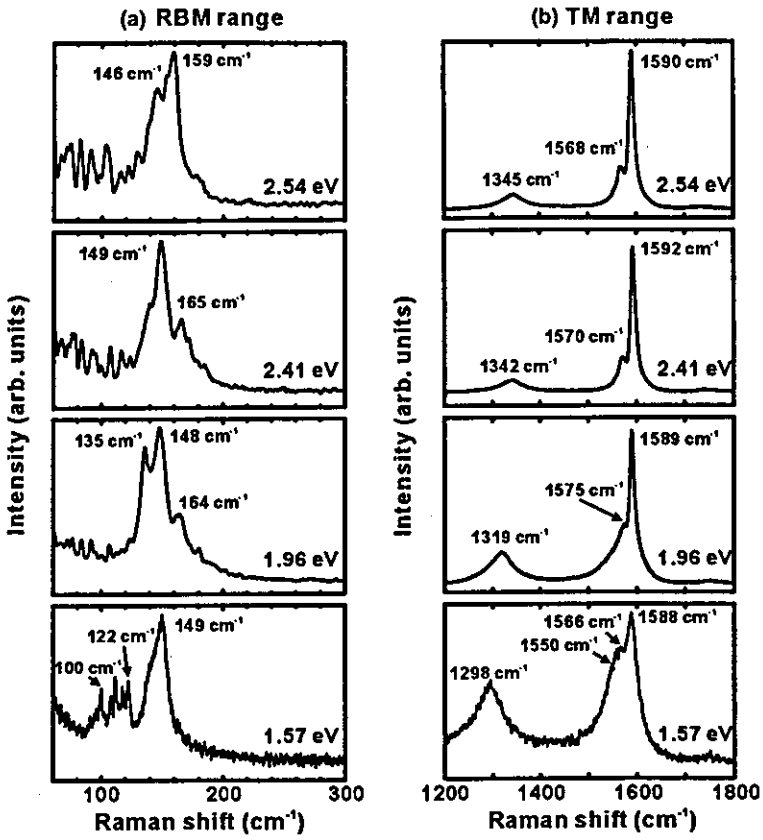

Fig. 3. Raman spectra in (a) RBM and (b) TM ranges using exciting laser with various photon energies for the soot synthesized at Ce concentration of 1.7 at.%, He 500 Torr and arc-discharge current of 70 A and subsequently burned in the air at 533 K for 1 h.

and a shoulder around 1550 cm^{-1} was observed. According to the relationship between diameter and the allowed optical transitions (transfer integral 2.9 eV) derived from band structure calculation based on the tight binding approximation [13,26], a SWCNT with a diameter of 1.5–1.6 nm will be exited by the incident light with energies 1.96, 2.41 and 2.54 eV only when the nanotube is a semiconductor. On the other hand, the metallic nanotube will be exited by an incident light of 1.57 eV. In the TM range, the shape of Raman spectra depends on the laser energy [27–29] and the splitting of the spectra into narrow and symmetric lines is assigned to the resonance from semiconducting SWCNTs, while the broad and asymmetric BFW lineshape type peak [13,30] that centered around 1550 cm^{-1} was assigned to the resonance from the metallic SWCNTs. Therefore, the broad lineshape around 1550 cm^{-1} was due to the presence of metallic SWCNTs.

UV–Vis–NIR spectroscopy is an established technique for characterizing the electronic band structure of SWCNTs [13,14,31–34]. Fig. 4 shows the UV–Vis–NIR spectrum of the soot synthesized at a Ce concentration of 1.7 at.%, He gas pressure of 500 Torr and arc-discharge current of 70 A and subsequently burned in air at 533 K for 1 h. The three peaks at 0.64, 1.14 and 1.60 eV were identified after the strong background due to π electron plasmon of two-dimensional carbon was subtracted from the raw data (inset in Fig. 4). By comparing the peak positions with the values calculated based on the zone folding method [26], these features

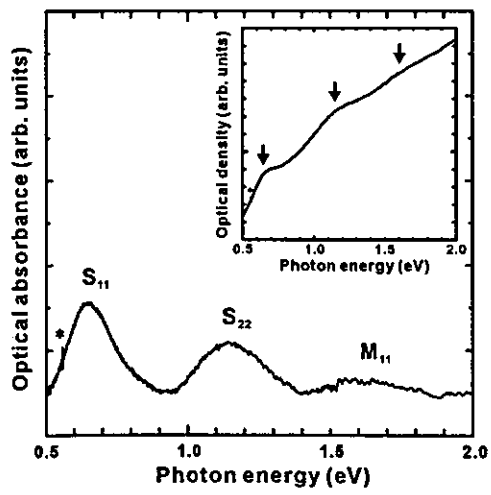

Fig. 4. UV–Vis–NIR spectrum of the soot synthesized at Ce concentration of 1.7 at.%, He 500 Torr and arc-discharge current of 70 A and subsequently burned in the air at 533 K for 1 h. Inset shows the raw UV–Vis–NIR spectrum. Asterisk (*) indicates absorption peak due to the quartz substrate.

were assigned to the allowed optical transitions (transfer integral 2.9 eV) between Van Hove singularities of the density of states in the SWCNT with a diameter of 1.5–1.6 nm. The peaks at 0.64 and 1.14 eV were attributed to the electronic transitions between pairs of singularities in semiconducting SWCNTs ($V_s^1 \rightarrow C_s^1$ and $V_s^2 \rightarrow C_s^2$, respectively), whereas the peak at about 1.60 eV was predominantly from the first pair of singularities ($V_m^1 \rightarrow C_m^1$) in metallic SWCNTs. The appearance of the absorbed energy of the M_{11} band appears at about 1.60 eV confirmed the presence of metallic SWCNTs. This result was in good agreement with the electronic band structure of SWCNTs measured from the Raman scattering spectra. The reason for its appearance at a higher-energy side compared to the calculated S_{11} is due to the Coulomb interaction between SWCNTs [35].

4. Conclusion

We have succeeded in improving the production efficiency of the radial SWCNTs to a value as high as about 20% (by volume from visual inspection of TEM images) using 1.7 at.% of Ce in anode, He gas pressure of 500 Torr and arc-discharge current of 70 A. From the TEM measurement and radial breathing mode of Raman spectra, the average length and diameter of the SWCNTs were determined to be 60 and 1.55 nm, respectively. Also, we have clarified the nature of the electronic structure of the radial SWCNTs. The presence of the metallic and semiconductor type SWCNTs was confirmed from the UV–Vis–NIR spectrum and the tangential mode of Raman spectra. In the carbon materials, conducting amorphous carbon has played an important role on the composites such as the electrode, conducting paints and conducting rubber. The nanotube-filler used in these applications is required to be conducting and easy to disperse in polymer and the nanotubes could be used to form the conducting channel within the polymer. The radial SWCNTs are more easily dispersed in polymer than the semi-finite long SWCNTs. We believe that the radial SWCNTs are applied as the conducting filler.

Acknowledgements

This work was supported by Grant-in-Aid for Basic Research #(S) 14103016 and #(S) 13852016 from the Ministry of Education, Science, Culture and Sport of Japan and #H14-nano-021 from the Ministry of Health, Labor and Welfare. The authors thank Mr. K. Motomiya of Tohoku University, Dr. T. Kamino and Dr. T. Yaguchi of Hitachi Science Systems, Ltd. for their assistance in HRTEM analysis. Y. S. thanks Dr. T. Takenobu of Institute for Materials Research, Tohoku University for useful information and Prof. A. Narayanasamy of University of Madras and Dr. C. N. Chinnasamy of Tohoku University for useful discussion. Also, the authors thank Dr. T. Kochi and Dr. S. Okamoto of HORIBA, Ltd. for the measurement of Raman scattering spectrum and Dr. Yamada of Hitachi Science Systems, Ltd. for the measurement of UV–Vis–NIR spectrum.

References

[1] S. Iijima, T. Ichihashi, Nature 363 (1993) 603.
[2] D.S. Bethune, C.H. Kiang, M.S. de Vries, G. Gorman, R. Savoy, J. Vazquez, R. Beyers, Nature 363 (1993) 605.
[3] A. Thess, R. Lee, P. Nikolaev, H. Dai, P. Petit, J. Robert, C. Xu, Y.H. Lee, S.G. Kim, A.G. Rinzler, D.T. Colbert, G.E. Scuseria, D. Tománek, J.E. Fischer, R.E. Smalley, Science 273 (1996) 483.
[4] K. Tohji, T. Goto, H. Takahashi, Y. Shinoda, N. Shimizu, B. Jeyadevan, I. Matsuoka, Y. Saito, A. Kasuya, T. Ohsuna, K. Hiraga, Y. Nishina, Nature 383 (1996) 679.
[5] J.L. Andrew, G. Rinzler, H. Dai, J.H. Hafner, R.K. Bradley, P.J. Boul, A. Lu, T. Iverson, K. Shelimov, C.B. Huffman, F. Rodriguez-Macias, Y.S. Shon, T.R. Lee, D.T. Colbert, R.E. Smalley, Science 280 (1998) 1253.
[6] R.H. Baughman, A.A. Zakhidov, W.A. de Heer, Science 297 (2002) 787.
[7] S.J. Tans, M.H. Devoret, H. Dai, A. Thess, R.E. Smalley, L.J. Geerligs, C. Dekker, Nature 386 (1997) 474.
[8] H. Dai, Acc. Chem. Res. 35 (2002) 1035.
[9] A. Modi, N. Koratkar, E. Lass, B. Wei, P.M. Ajayan, Nature 424 (2003) 171.
[10] R. Saito, G. Dresselhaus, M.S. Dresselhaus, Physical Properties of Carbon Nanotubes, Imperial College Press, London, 1998.
[11] S. Niyogi, M.A. Hamon, H. Hu, B. Zhao, P. Bhowmik, R. Sen, M.E. Itkis, R.C. Haddon, Acc. Chem. Res. 35 (2002) 1105.
[12] M.F. Yu, B.S. Files, S. Arepalli, R.S. Ruoff, Phys. Rev. Lett. 84 (2000) 5552.
[13] H. Kataura, Y. Kumazawa, Y. Maniwa, I. Umezu, S. Suzuki, Y. Ohtsuka, Y. Achiba, Synth. Met. 103 (1999) 2555.
[14] H. Kuzmany, W. Plank, M. Hulman, C. Kramberger, A. Grüneis, T. Pichler, H. Peterlik, H. Kataura, Y. Achiba, Eur. Phys. J. B 22 (2001) 307.
[15] S. Subramoney, R.S. Ruoff, D.C. Lorents, R. Malhotra, Nature 366 (1993) 637.
[16] D. Zhou, S. Seraphin, S. Wang, Appl. Phys. Lett. 65 (1994) 1593.
[17] Y. Saito, K. Kawabata, M. Okuda, J. Phys. Chem. 99 (1995) 16076.
[18] L. Alvarez, T. Guillard, J.L. Sauvajol, G. Flamant, D. Laplaze, Appl. Phys. A 70 (2000) 169.
[19] A. Kasuya, Y. Sasaki, Y. Saito, K. Tohji, Y. Nishina, Phys. Rev. Lett. 78 (1997) 4434.
[20] L. Alvarez, A. Righi, T. Guillard, S. Rols, E. Anglaret, D. Laplaze, J.L. Sauvajol, Chem. Phys. Lett. 316 (2000) 186.
[21] C.G. Suits, J. Appl. Phys. 10 (1939) 728.
[22] W. Finkelnburg, J. Appl. Phys. 20 (1949) 468.
[23] A.L. Phillips (Ed.), Welding Handbook, sixth ed., American Welding Society, New York, 1968 (Sec.1, Chapter 3).
[24] L. Alvarez, T. Guillard, J.L. Sauvajol, G. Flamant, D. Laplaze, Chem. Phys. Lett. 324 (2001) 7.
[25] S.M. Bachilo, M.S. Strano, C. Kittrell, R.H. Hauge, R.E. Smalley, R.B. Weisman, Science 298 (2002) 2361.
[26] S.D.M. Brown, P. Corio, A. Marucci, M.A. Pimenta, M.S. Dresselhaus, G. Dresselhaus, Phys. Rev. B 61 (2000) 7734.

[27] A. Kasuya, M. Sugano, T. Maeda, Y. Saito, K. Tohji, H. Takahashi, Y. Sasaki, M. Fukushima, Y. Nishina, C. Horie, Phys. Rev. B 57 (1998) 4999.
[28] M. Sugano, A. Kasuya, K. Tohji, Y. Saito, Y. Nishina, Chem. Phys. Lett. 292 (1998) 575.
[29] M.A. Pimenta, A. Marucci, S.A. Empedocles, M.G. Bawendi, E.B. Hanlon, A.M. Rao, P.C. Eklund, R.E. Smalley, G. Dresselhaus, M.S. Dresselhaus, Phys. Rev. B 58 (1998) 16016.
[30] Z. Yu, L. Brus, J. Phys. Chem. B 105 (2001) 1123.
[31] J. Chen, M.A. Hamon, H. Hu, Y. Chen, A.M. Rao, P.C. Eklund, R.C. Haddon, Science 282 (1998) 95.
[32] M.E. Itkis, S. Niyogi, M.E. Meng, M.A. Hamon, H. Hu, R.C. Haddon, Nano Lett. 2 (2002) 155.
[33] P. Petit, C. Mathis, C. Journet, P. Bernier, Chem. Phys. Lett. 305 (1999) 370.
[34] S. Kazaoui, N. Minami, R. Jacquemin, H. Kataura, Y. Achiba, Phys. Rev. B 60 (1999) 13339.
[35] M. Ichida, S. Mizuno, Y. Tani, Y. Saito, A. Nakamura, J. Phys. Soc. Jpn. 68 (1999) 3131.